JOURNAL OF THE AMERICAN CHEMICAL SOCIETY

Communication

pubs.acs.org/JACS

Unveiling Chemical Reactivity and Structural Transformation of Two-Dimensional Layered Nanocrystals

Jae Hyo Han,[†] Sujeong Lee,[†] Dongwon Yoo,[†] Jae-Hyun Lee,[†] Sohee Jeong,[†] Jin-Gyu Kim,[‡] and Jinwoo Cheon*,[†]

[†]Department of Chemistry, Yonsei University, Seoul 120-749, Korea

[‡]Division of Electron Microscopic Research, Korea Basic Science Institute, Daejeon 305-333, Korea

Supporting Information

ABSTRACT: Two-dimensional (2D) layered nanostructures are emerging fast due to their exceptional materials properties. While the importance of physical approaches (e.g., guest intercalation and exfoliation) of 2D layered nanomaterials has been recognized, an understanding of basic chemical reactions of these materials, especially in nanoscale regime, is obscure. Here, we show how chemical stimuli can influence the fate of reaction pathways of 2D layered nanocrystals. Depending on the chemical characteristics (Lewis acid ($^1O_2$) or base (H_2O)) of external stimuli, TiS_2 nanocrystal is respectively transformed to either a TiO_2 nanodisc through a "compositional metathesis" or a TiO_2 toroid through multistage "edge-selective structural transformation" processes. These chemical reactions can serve as the new design concept for functional 2D layered nanostructures. For example, $TiS_{2(disc)}$-$TiO_{2(shell)}$ nanocrystal constitutes a high performance type II heterojunction which not only a wide range solar energy coverage (~80%) with near-infrared absorption edge, but also possesses enhanced electron transfer property.

Two-dimensional (2D) layered nanostructures, existing in diverse chemical compositions and crystal structures have drawn huge interest from academia and industry because of their extraordinary materials properties and wide range of potential applications.[1] In conjunction with weak van der Waals interactions between the layers, top-down physical approaches have been widely utilized for intercalations of guest molecules or exfoliations of multiple layers into single layer sheets.[1b,c] Despite the potential importance of chemical approaches for tailoring materials properties and enhancing performance, very little, especially in nanoscale regime, is known for 2D layered transition metal chalcogenide (TMC) nanocrystals, whereas evidence are already shown for graphene where surface oxidation, edge passivation and molecular functionalization are essential to satisfy desired materials properties.[2] Unlike graphene, TMCs possess transition metal based d-electrons that can be advantageous to modulate wide variety of materials properties. For example, single layer molybdenum disulfide (MoS_2) is fascinating due to the possession of direct band gap that is critical for applications in optoelectronics and energy harvesting.[3]

Scheme 1. Chemical Stimuli Driven Compositional Metathesis and Edge-Selective Reaction of 2D Layered Nanocrystal

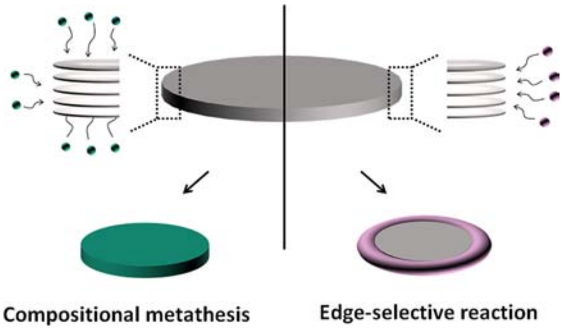

Herein, we explored unique nanoscale phenomena, including a "compositional metathesis" and a regioselective "morphological transformation", promoted by subjecting 2D layered TMC nanocrystals to chemical stimuli (Scheme 1). Since acid and base are the most fundamental chemical characteristics, we choose to test their reactions with 2D layered titanium disulfide (TiS_2) nanocrystals as an exemplary for understanding of their nanoscale chemical reactivity. TiS_2 nanocrystals are exposed to either oxygen (O_2) or water (H_2O): more specifically (i) singlet oxygen ($^1O_2$) as an electrophilic Lewis acid[4] and (ii) water as a nucleophilc Lewis base that donates electrons[5]. We demonstrate that these two chemical stimuli convert layered TiS_2 into titanium dioxide (TiO_2) as a final product, but via markedly different reaction pathways with distinct nanoscale morphologies.

As a first step, the response of TiS_2 nanocrystals upon exposure to O_2 is investigated. Single-crystalline TiS_2 nanodisc employed in this study is 150 nm ($\sigma \approx 15\%$) in diameter with a thickness of ca. 10 nm (Figure 1a).[6] The (001) lattice plane held by van der Waals interaction is 5.7 Å, a characteristic distance between units composed of S−Ti−S triatomic layers (Figure 1b,c). A diluted O_2/Ar (3:7 in volume) gas is continuously blown to a heated colloidal solution of TiS_2 nanocrystals (1.5 mg/mL) in oleylamine at 140 °C (Figure 1d). Heating (>120 °C) is necessary for the generation of chemically reactive $^1O_2$ (vide infra).[7] Figure 1e shows the TEM images where changes from clean discs ((i), 0 h) to multiple dots embedded within discs

Received: October 4, 2012
Published: March 4, 2013

dx.doi.org/10.1021/ja309744c | J. Am. Chem. Soc. 2013, 135, 3736−3739

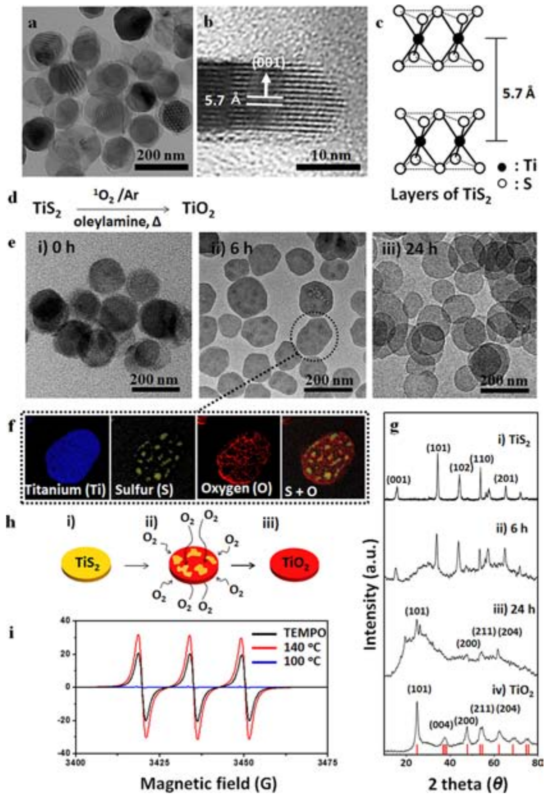

Figure 1. Disc to disc compositional metathesis (S to O) reaction driven by Lewis acid ($^1O_2$). (a) Low-magnification TEM image of disc-shaped TiS_2 nanocrystals. (b) High-resolution TEM side-view image. Each layer is separated by weak van der Waals interaction and the distance between the metals is 5.7 Å. (c) Layer structure of TiS_2 (Ti, dark circle; S, open circle). (d) The reaction of TiS_2 upon $^1O_2$ as chemical stimulus. (e) TEM images of TiS_2 nanocrystals treated with $^1O_2$ for (i) 0 h, (ii) 6 h and (iii) 24 h. Note that dark contrast dots appear in (ii), but are absent in (iii). (f) EELS analysis of nanocrystals collected at 6 h (Ti, blue; S, yellow; O, red). Sulfur containing dots (TiS_2) are surrounded by oxygen (TiO_2). (g) XRD patterns of TiS_2 and transformed nanocrystals (i) 0 h (TiS_2), (ii) 6 h, (iii) 24 h and (iv) thermally treated (iii) at 500 °C. (h) A schematic diagram of disc to disc compositional metathesis of TiS_2 to TiO_2. (i) EPR spectra of 2,2,6,6-tetramethyl-1-piperidine (TEMP) solution exposed to O_2 at 100 (blue) and 140 °C (red), respectively. 2,2,6,6-Tetramethylpiperidine oxide (TEMPO) used as radical generation control (black).

((ii), 6 h) are observed. As the reaction further proceeds, dots disappear, but the disc morphology with an almost identical size compared to the starting material is preserved ((iii), 24 h). The results of elemental analysis using electron energy loss spectroscopy (EELS) (Figure 1f) indicate that the embedded dots in the intermediate stage are TiS_2, which is consistent with moderate intensity peaks of TiS_2 observed in X-ray diffraction (XRD) patterns (Figure 1g (ii)). Discs at 24 h show, with disappearance peaks of TiS_2, new peaks with weak intensities for (101), (200), (211), and (204) of anatase structure along with very broad peaks indicating the existence of mixture of crystalline and amorphous TiO_2 (Figure 1g (iii)). Thermal treatment (500 °C) of discs formed at 24 h confirms crystalline anatase structure (Figure 1g (iv)) (JCPDS 21-1272). Overall, exposure of TiS_2 to O_2 promotes a complete conversion of a TiS_2 disc to a TiO_2 disc without noticeable change of its shape and size, which implies that the reaction takes place via "compositional metathesis".

We also tested the chemical reactivity of TiS_2 nanocrystals with H_2O. TiS_2 nanocrystals (5 mg) are dispersed and stirred in a mixture of toluene (3 mL) and H_2O (0.3 mL) at room temperature (Figure 2a). During the initial stage at 12 h, clean edge of a disc turns to a shell (~20 nm) with a slight contrast difference in TEM images (Figure 2b (i and ii)). The chemical compositional analysis using EELS indicates that the edge of the disc is transformed to the oxide (red) while the core remains TiS_2 (Figure 2e) with a $TiS_{2(disc)}$-$TiO_{2(shell)}$ structure. As the reaction further proceeds, a $TiS_{2(disc)}$-$TiO_{2(toroid)}$ structure with thin gaps (~3−5 nm) at their interfaces is observed at 36 h (Figure 2b (iii)). Eventually, this intermediate structure changes to a toroid at 60 h (Figure 2b (iv)). In the XRD pattern (Figure 2g), the gradual decreases of TiS_2 peaks take place along the steady growth of a broad peak centered at $2\theta = \sim 20°$ (Figure 2g (iv)). The broad peak is occasionally observed in sol−gel mediated TiO_2 formation, indicating therefore the growth of amorphous TiO_2 at the edge of disc.[8] Upon thermal treatment of the toroid nanocrystals at 500 °C, pure anatase structure is obtained (Figure 2g (v)) (JCPDS 21-1272). While the size of TiS_2 continuously decreases from 150 to 60 nm and eventually disappears to create a void (Figure 2b), the total diameter of disc expands from 150 to 180 nm and then remains constant from stage iii to iv (Figure 2f).

Distinctly different chemical reactions of TiS_2 upon exposure to O_2 and H_2O are largely attributed by its unique 2D layered structural and compositional anisotropy, with the basal plane being completely covered with S atoms and edges containing partially coordinated Ti and S atoms.[9] When exposed to this singlet oxygen, oxidation by electrophilic singlet oxygen ($^1O_2$) of the electron rich sulfur ions (S^{2-})[10] on the basal surfaces, edges and between the layers throughout the TiS_2 discs is possible (Figure 1h). As a result, "compositional metathesis" occurs in the formation of TiO_2. Temperature dependent formation of singlet oxygen is separately confirmed by detecting oxidized TEMPO by EPR spectroscopy (Figure 1i).[11] Nitroxide radical of TEMPO is detected only at the elevated temperature (e.g., 140 °C) whereas negligible amount of radical is observed at low temperatures (e.g., 100 °C). These EPR results indicate that singlet oxygen is generated adequately at 140 °C to promote the oxidation reaction (Figures S1 and S2). In contrast to the case of O_2, regioselective edge initiated shape transformation is promoted by the nucleophilc chemisorption of H_2O toward titanium atoms exposed on the edges (Figure 2d).[12] Via a sol−gel process, the formation of Ti hydroxide derivatives, $Ti(OH)_{4-x}$ ($x = 1-3$), and polycondensation processes are expected to have amorphous TiO_2.[13] The nanoscale void formation between TiS_2−TiO_2 is a unique signature of operation of the diffusion of Ti^{4+} ions via vacancy exchange process.[14] The relationship between reaction time vs temperature shows exponential decrease in reaction time as temperature increases, which fits well with the plot estimated by Kirkendall theory (Figures S3 and S4). Once the gap widens, then inward growth occurs from the gap with the expense of TiS_2, which eventually leads to the formation of TiO_2 toroid (Figure 2c).

Such regioselective chemical transformation upon exposure to H_2O is fascinating since it can permit the modulation of physical and chemical properties of 2D layered nanocrystals. As an example, optical property of TiS_2 nanocrystal is of interest. In the absorption spectrum, TiS_2 nanocrystal shows a peak at ~650 nm and a shoulder at ~1350 nm (Figure 3a) that are assigned as M and Γ transitions.[15] The TiS_2 nanocrystal band gap energy of 0.66 eV (Figure S5) is blue-shifted from that of the bulk material.[16] As the oxidation on the edge of TiS_2 progresses to $TiS_{2(disc)}$-$TiO_{2(shell)}$ and $TiS_{2(disc)}$-$TiO_{2(toroid)}$, M transition consistently shifts from 655 to 630 and 590 nm (Figure 3a)

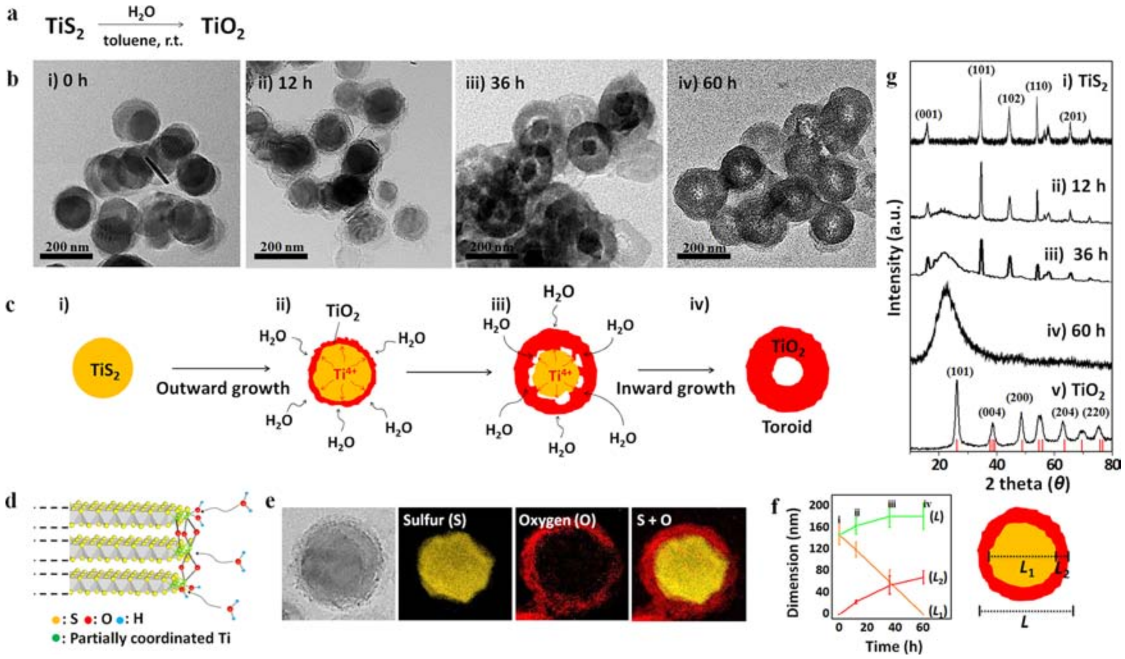

Figure 2. Disc to toroid TiO_2 morphological transformation driven by Lewis base (H_2O). (a) The reaction of TiS_2 upon H_2O as chemical stimulus. (b) TEM images at each transformation stage from TiS_2 nanodiscs to toroid TiO_2 nanocrystals by reacting TiS_2 with H_2O for (i) 0 h, (ii) 12 h, (iii) 36 h and (iv) 60 h. (i) $TiS_{2(disc)}$ transforms to (ii) $TiS_{2(disc)}$-$TiO_{2(shell)}$, (iii) $TiS_{2(disc)}$-$TiO_{2(toroid)}$ and (iv) $TiO_{2(toroid)}$. (c) A schematic diagram of morphological transformations of TiS_2. For stage (i→ii), chemisorption of nucleophile H_2O to titanium metals occurs on the edge surface of TiS_2. For stage (ii→iii), arrows are drawn to indicate that H_2O access Ti through both edges and exposed gaps between TiS_2 and TiO_2. For stage (iii→iv), inward growth of TiO_2 progresses. (d) A schematic illustration of chemisorption of H_2O molecules on titanium dangling bonds on the edge (S, yellow; partially coordinated Ti, green; O, red; H, blue), which is followed by hydrolysis and condensation reactions to create Ti−OH and Ti−O−Ti. (e) EELS analysis of intermediate (ii) $TiS_{2(disc)}$-$TiO_{2(shell)}$ nanocrystal (12 h). Sulfur is shown in yellow (disc) and oxygen in red (shell). (f) Plot showing the changes in size of TiS_2 (L_1), TiO_2 (L_2) and overall (L) nanocrystals. (g) XRD patterns of TiS_2 and transformed nanocrystals. (i) TiS_2 (0 h), (ii) 12 h, (iii) 36 h, (iv) 60 h, and (v) thermally treated (iv) at 500 °C.

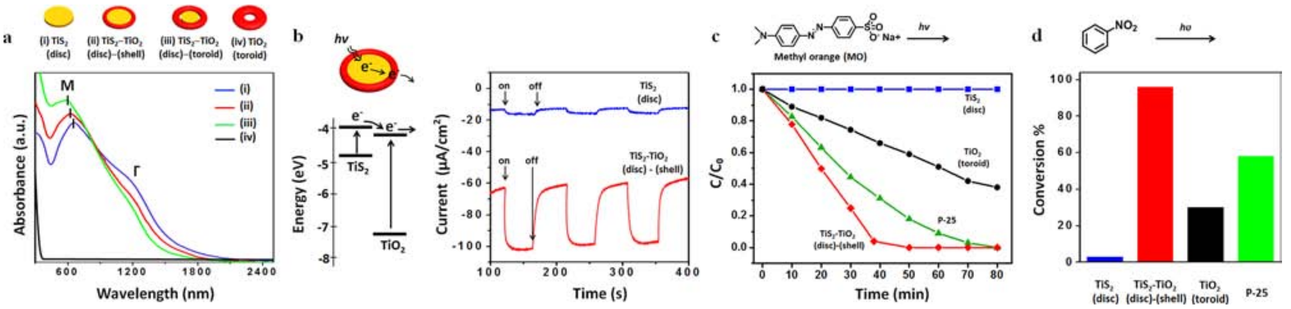

Figure 3. Optical and catalytic properties of TiS_2−TiO_2 nanocrystals. (a) Absorption spectra of (i) $TiS_{2(disc)}$ (blue), (ii) $TiS_{2(disc)}$-$TiO_{2(shell)}$ (red), (iii) $TiS_{2(disc)}$-$TiO_{2(toroid)}$ (green), and (iv) $TiO_{2(toroid)}$ (black) nanocrystals, respectively. (b) The energy band alignment of $TiS_{2(disc)}$-$TiO_{2(shell)}$ nanocrystals relative to vacuum level. The top illustration depicts transfer of photogenerated electrons of TiS_2 to the conduction band of TiO_2 and reductant. Photocurrent response of $TiS_{2(disc)}$ (blue) and $TiS_{2\ (disc)}$-$TiO_{2\ (shell)}$ (red) nanocrystals. (c) Comparison of photocatalytic activity of methyl orange (MO) degradation: $TiS_{2(disc)}$ (blue ■), $TiO_{2(toroid)}$ (black ●), P-25 (green ▲), and $TiS_{2\ (disc)}$-$TiO_{2(shell)}$ (red ◆) nanocrystals. (d) Comparison of photocatalytic reduction efficiency of nitrobenzene by $TiS_{2(disc)}$ (blue), $TiS_{2(disc)}$-$TiO_{2(shell)}$ (red), $TiO_{2(toroid)}$ (black) and P-25 (green) conducted at 298 K in methanol for 2 h.

that is likely caused by size reduction of TiS_2 from 150 nm to 110 and 60 nm in respective structure (Figure 2f).[17] Without any TiS_2 component, TiO_2 toroid gives typical absorption starting around 390 nm (Figure 3a).

More importantly, we discovered that $TiS_{2(disc)}$-$TiO_{2(shell)}$ nanocrystals offer enhanced solar energy uptake and facilitated electron transfer properties. The LUMO energy level of anatase TiO_2 is −4.2 eV[18] and the respective HOMO and LUMO energies of TiS_2 are determined to be −4.7 and −4.0 eV by cyclic voltammetry (Figure S6). Thus, the staggered band alignment of the $TiS_{2(disc)}$-$TiO_{2(shell)}$ creates type II heterojunction (Figure 3b) that the amount of photocurrent generated by $TiS_{2(disc)}$-$TiO_{2(shell)}$ nanocrystals is significantly larger than that by $TiS_{2(disc)}$ where the current is barely observed. The observation suggests that smooth electron transport from TiS_2 to TiO_2 without significant decay of photogenerated electrons of TiS_2 (Figure 3b). Because functionalized $TiS_{2(disc)}$-$TiO_{2(shell)}$ nanocrystals exhibit enhanced charge separation, it may act as efficient solar energy harvesting material. As a proof-of-concept study, we examined $TiS_{2(disc)}$-$TiO_{2(shell)}$ nanocrystals for its photocatalytic activity (Figure 3c). Three different nanocrystals ($TiS_{2(disc)}$, $TiS_{2(disc)}$-$TiO_{2(shell)}$ and $TiO_{2(toroid)}$) and Degussa P-25 are added to a 100 mL of aqueous solution containing 2×10^{-5} M of methyl orange (MO).[19a] While TiS_2 nanodiscs show almost no photocatalytic activity (i.e., MO remained unchanged) and $TiO_{2(toroid)}$ decomposes 28% of MO, $TiS_{2(disc)}$-$TiO_{2(shell)}$ nanocrystals completely degrade MO under illumination of 150 W Tungsten lamp for 40 min. In case of Degussa P-25, it takes approximately 78 min for complete degradation. Similar efficiency is also observed in the photocatalytic reduction of nitrobenzene (NB) (Figure 3d).[19b] $TiS_{2(disc)}$-$TiO_{2(shell)}$ nanocrystals completely reduce NB whereas $TiO_{2(toroid)}$ and Degussa P-25 convert 35% and 58% of NB, respectively. The low photocatalytic activity of pure TiS_2 nanocrystals is expected based on the fact that the fast charge recombination rate of narrow band gap semiconductor and the presence of trap sites on the edges.[20] Meanwhile, $TiS_{2(disc)}$-$TiO_{2(shell)}$ nanocrystals show highest conversion efficiency which is attributed by its capability to absorb wide spectral region. In fact, the band edge of $TiS_{2(disc)}$-$TiO_{2(shell)}$ nanocrystals starts from near-infrared (~1620 nm, 0.76 eV) and covers the entire visible region, which corresponds to ~80% of available solar spectrum.[21] This value well exceeds thus far reported type II metal chalcogenide-oxide hybrid nanocrystals such as PbS-, CdSe- and WS_2-TiO_2.[22] The high biocompatibility of titanium for health and environment and also its large abundance only next to iron are advantageous. In addition, the high absorption coefficient ($>10^4$ cm^{-1} in the IR region)[23] of TiS_2 and the large carrier mobility attributed by 2D layered structure[24] are beneficial for the use in solar energy harvesting applications.

By introducing the basic concepts of chemical principles, we observed new possibilities for expanding the science of 2D layered TMCs where appropriate selection of chemical stimulus is critical to drive structural changes from simple to complex nanostructures with fine-tuned materials properties. Given that, our study constitutes a new finding for unique chemical principles correlated with the high anisotropy of 2D layered TMCs. Since this approach can, in principle, be applied to a variety of 2D layered nanostructures ranging from TMC nanocrystals to topological insulators and thermoelectric materials, we anticipate new outcomes of structurally diverse and functionally enhanced 2D layered nanostructure through better understanding of chemistry.

■ ASSOCIATED CONTENT

Ⓢ Supporting Information

Details of synthetic methods and characterizations, theoretical calculation on Kirkendall theory, band gap energy calculation, cyclic voltammetry and chemical reactions with other electrophile and nucleophile. This material is available free of charge via the Internet at http://pubs.acs.org.

■ AUTHOR INFORMATION

Corresponding Author

jcheon@yonsei.ac.kr

Notes

The authors declare no competing financial interest.

■ ACKNOWLEDGMENTS

This study was carried out with the financial support of the Creative Research Initiative (2010-0018286), WCU (R32-10217) and KBSI-HVEM (JEM-ARM 1300S). We thank N. H. Kim and S. H. Kim at KBSI for EPR analyses and Prof. Dongil Lee at Yonsei Univ. for helpful discussion and electrochemical measurements.

■ REFERENCES

(1) (a) Geim, A. K. *Science* **2009**, *324*, 1530. (b) Morosan, E.; Zandbergen, H. W.; Dennis, B. S.; Bos, J. W. G.; Onose, Y. *Nat. Phys.* **2006**, *2*, 544. (c) Wang, Q. H.; Kalantar-Zadeh, K.; Kis, A.; Coleman, J. N.; Strano, M. S. *Nat. Nanotechnol.* **2012**, *7*, 699. (d) Novoselov, K. S.; Geim, A. K.; Morozov, S. V.; Jiang, D.; Zhang, Y.; Dubonos, S. V.; Grigorieva, I. V.; Firsov, A. A. *Science* **2004**, *306*, 666. (e) Han, J.; Lee, S.; Cheon, J. *Chem. Soc. Rev.* **2013**, DOI: 10.1039/C2CS35386E.

(2) (a) Dreyer, D. R.; Park, S.; Bielawski, C. W.; Ruoff, R. S. *Chem. Soc. Rev.* **2010**, *39*, 228. (b) Liu, L.; Ryu, S.; Tomasik, M. R.; Stolyarova, E.; Jung, N.; Hybertsen, M. S.; Steigerwald, M. L.; Brus, L. E.; Flynn, G. W. *Nano Lett.* **2008**, *8*, 1965. (c) Wheling, T. O.; Novoselov, K. S.; Morozov, S. V.; Vdovin, E. E.; Katsnelson, M. I.; Geim, A. K.; Lichtenstein, A. I. *Nano Lett.* **2008**, *8*, 173.

(3) (a) Radisavljevic, B.; Radenovic, A.; Brivio, J.; Giacometti, V.; Kis, A. *Nat. Nanotechnol.* **2011**, *6*, 147. (b) Chianelli, R. R.; Siadati, M. H.; De la Rosa, M. P.; Berhault, G.; Wilcoxon, J. P.; Bearden, R., Jr.; Abrams, B. L. *Catal. Rev.* **2006**, *48*, 1.

(4) Ochiai, E. *Bioinorganic Chemistry: A Survey*, 1st ed.; Academic Press: Boston, MA, 2008; Charter 6.

(5) Piera, J.; Persson, A.; Caldentey, X.; Bäckvall, J.-E. *J. Am. Chem. Soc.* **2007**, *129*, 14120.

(6) Jeong, S.; Han, J.; Jang, J.-t.; Seo, J.-w.; Kim, J.-G.; Cheon, J. *J. Am. Chem. Soc.* **2011**, *133*, 14500.

(7) Romanov, A. N.; Bykhovskii, M. Y.; Rufov, Y. N.; Korchak, V. N. *Kinet. Catal.* **2000**, *41*, 782.

(8) Cozzoli, P. D.; Kornowski, A.; Weller, H. *J. Am. Chem. Soc.* **2003**, *125*, 14539.

(9) Jaegermann, W.; Schmeisser, D. *Surf. Sci.* **1986**, *165*, 143.

(10) Martinez, H.; Auriel, C.; Gonbeau, D.; Loudet, M.; Pfister-Guillouzo, G. *Appl. Surf. Sci.* **1996**, *93*, 231.

(11) Yamakosh, Y.; Umezawa, N.; Ryu, A.; Arakane, K.; Miyata, N.; Goda, Y.; Masumizu, T.; Nagano, T. *J. Am. Chem. Soc.* **2003**, *125*, 12803.

(12) Sun, C.; Liu, L.-M.; Selloni, A.; Lu, G. Q.; Smith, S. C. *J. Mater. Chem.* **2010**, *20*, 10319.

(13) Li, G.; Li, L.; Boerio-Goates, J.; Woodfield, B. F. *J. Am. Chem. Soc.* **2005**, *127*, 8659.

(14) Son, D. H.; Hughes, S. M.; Yin, Y.; Alivisatos, A. P. *Science* **2004**, *306*, 1009.

(15) Beal, A. R.; Knights, J. C.; Liang, W. Y. *J. Phys. C: Solid State Phys.* **1972**, *5*, 3531.

(16) Fang, C. M.; de Groot, R. A.; Hass, C. *Phys. Rev. B* **1997**, *56*, 4455.

(17) Liu, Y.-H.; Porter, S. H.; Goldberger, J. E. *J. Am. Chem. Soc.* **2012**, *134*, 5044.

(18) Kubacka, A.; Fernández-García, M.; Colón, G. *Chem. Rev.* **2011**, *112*, 1555.

(19) (a) Liu, S.; Yu, J.; Jaroniec, M. *J. Am. Chem. Soc.* **2010**, *132*, 11914. (b) Flores, S. O.; Rios-Bernij, O.; Valenzuela, M. A.; Córdova, I.; Gómez, R.; Gutiérrez, R. *Top. Catal.* **2007**, *4*, 507.

(20) Tributsch, H. *Faraday Discuss. Chem. Soc.* **1980**, *70*, 189.

(21) Unold, T.; Schock, H. W. *Annu. Rev. Mater. Res.* **2011**, *41*, 297.

(22) (a) Acharya, K. P.; Hewa-Kasakarage, N. N.; Alabi, T. R.; Nemitz, I.; Khon, E.; Ullrich, B.; Anzenbacher, P.; Zamkov, M. *J. Phys. Chem. C* **2010**, *114*, 12496. (b) Kongkanand, A.; Tvdy, K.; Takechi, K.; Kuno, M.; Kamat, P. V. *J. Am. Chem. Soc.* **2008**, *130*, 4007. (c) Tahir, M. N.; Zink, N.; Eberhardt, M.; Therese, H. A.; Faiss, S.; Janshoff, A.; Kolb, U.; Theato, P.; Tremel, W. *Small* **2007**, *3*, 829.

(23) Lee, P. A.; Said, G.; Davis, R.; Lim, T. H. *J. Phys. Chem. Solids* **1969**, *30*, 2719.

(24) Imai, H.; Shimakawa, Y.; Kubo, Y. *Phys. Rev. B.* **2001**, *64*, 241104.